Available online at www.sciencedirect.com

ScienceDirect

Ceramics International 40 (2014) 3361–3369

CERAMICS INTERNATIONAL

www.elsevier.com/locate/ceramint

Hydroxyapatite nanofibers fabricated through electrospinning and sol–gel process

Jung-Hee Lee, Young-Jin Kim*

Department of Biomedical Engineering, Catholic University of Daegu, Gyeongsan 712-702, Republic of Korea

Received 25 April 2013; received in revised form 1 August 2013; accepted 22 September 2013
Available online 29 September 2013

Abstract

For the replacement and regeneration of hard tissues, hydroxyapatite (HA) has been considered to be one of the most promising biomaterials. To develop new potential HA-based nanofibers, microfibrous composite membranes were first prepared by electrospinning from gelatin–calcium phosphate (CaP) sol blend solutions of various concentrations of CaP sol. The resulting fibers exhibited a fully interconnected porous structure and their average diameter varied from 1.09 ± 0.24 μm to 1.44 ± 0.17 μm according to the CaP sol content. For the fabrication of HA nanofibers, the thermal treatment of microfibrous composite membrane was carried out. After the thermal treatment at 800 °C, the average fiber diameter of GECP20 composite membrane significantly reduced from 1.21 ± 0.21 μm to 400 ± 52 nm, which may be caused by the elimination of gelatin due to the thermal treatment. ATR-FTIR, EDX, XRD and XRF analyses confirmed that the HA nanofibers could be produced by combining the electrospinning and thermal treatment methods in the sol–gel process. These HA nanofibers showed the same crystalline phase with that of the stoichiometric HA. In addition, the results from simulated body fluid immersion (SBF) test and cell viability assay showed the improved in vivo bone bioactivity of HA nanofibers.

Keywords: A. Sol–gel processes; B. Fibers; D. Apatite; E. Biomedical applications

1. Introduction

Hydroxyapatite (HA) belongs to a class of calcium phosphate based materials. Due to its biocompatibility, osteoconductivity and bioactivity, HA has long been widely used in medical and dental applications as a material for damaged bones or teeth, important implant and scaffold materials and as a drug delivery agent [1–3]. Synthetic HA exhibits strong affinity to host hard tissue because of the chemical similarity between HA and mineralized bone of human tissue. Formation of chemical bonds with the host tissue offers HA a greater advantage in clinical applications than most other bone substitutes such as allografts or metallic implants.

Among the different techniques available for the production of HA, the sol–gel process is the simplest and most versatile, which is generally based on hydrolysis reactions followed by the condensation of the precursors to achieve the formation of colloidal particles (sol) and the subsequent formation of a three-dimensional network (gel) [4]. Through this technique it is possible to produce powders and fibers of HA with sub-micron dimensions.

HA-based nanofibrous scaffolds are particularly promising to use as a variety of implantable materials such as bone blocks and defect fillers in order to support cell functions and to stimulate regeneration of new tissues [5]. Various methods have been developed to fabricate porous HA scaffolds including the incorporation of volatile organic particles, gel casting and salt leaching [6–8]. Recently, several researchers have used electrospinning for the production of microfibrous ceramic structures containing a network of sub-micron fibers [5,9]. In this case, the sol is generally electrospun with a polymer solution and the resultant structure is calcined at high temperatures to remove the polymer. However, these electrospun HA fibers showed mixture forms containing calcium oxide and tricalcium phosphate and were not fully characterized.

The electrospinning technique is an effective means to produce a nonwoven membrane of nanofibers from a variety of polymer and composite materials. In addition, the sol–gel technique has provided new opportunities for the preparation

*Corresponding author. Tel.: +82 53 850 2512; fax: +82 53 850 2510.
E-mail address: yjkim@cu.ac.kr (Y.-J. Kim).

0272-8842/$ - see front matter © 2013 Elsevier Ltd and Techna Group S.r.l. All rights reserved.
http://dx.doi.org/10.1016/j.ceramint.2013.09.096

of organic–inorganic composite materials, which allows the formation of inorganic network under mild condition [10]. In this study, a new method for the production of HA nanofibers was developed by combining the electrospinning and thermal treatment methods for use in the sol–gel process. The objective of this work was to prepare the HA nanofibers. With their high area to volume ratio, HA nanofibers are expected to be excellent materials for biomedical applications. The prepared HA nanofibers were systematically examined by considering their morphologies, chemical structures, crystalline phases and thermal properties. Moreover, the ability of bone-like apatite formation on the surface of HA nanofibers by immersion in simulated body fluid (SBF) was evaluated. In addition, the cytocompatibility of HA nanofibers was evaluated by assaying cell proliferation.

2. Experimental

2.1. Materials

Calcium nitrate tetrahydrate ($Ca(NO_3)_2 \cdot 4H_2O$), triethyl phosphite ($(C_2H_5O)_3P$), hydroxyapatite nanopowder, gelatin from cold water fish skin, 2,2,2-trifluoroethanol (TFE), calcium chloride anhydrous ($CaCl_2$) and ethanol were purchased from Sigma–Aldrich Co. (USA) and used without further purification. Minimum essential medium alpha (MEM-α), fetal bovine serum (FBS), phosphate buffered saline (PBS, pH 7.4) and penicillin–streptomycin were obtained from Gibco BRL (USA). Other reagents and solvents were commercially available and were used as received.

2.2. Synthesis of calcium phosphate sol

A synthesis of calcium phosphate (CaP) sol is as follows: $Ca(NO_3)_2 \cdot 4H_2O$ and $(C_2H_5O)_3P$ were used as raw materials for preparing the sol [5]. 14.0 g of $Ca(NO_3)_2 \cdot 4H_2O$ was dissolved in 10 mL of ethanol and 5.9 g of $(C_2H_5O)_3P$ was hydrolyzed with 10 mL of ethanol. The $Ca(NO_3)_2 \cdot 4H_2O$ solution was added dropwise into the $(C_2H_5O)_3P$ solution for 1 h to obtain a Ca/P ratio of 1.67. The mixture solution was stirred vigorously for 24 h at 40 °C and aged at 60 °C for 6 h. The resulting sol was evaporated for 1 h to increase the viscosity and to obtain the sol solution with a solid content of 80 w/v%.

2.3. Preparation of hydroxyapatite nanofibers

The electrospinning setup utilized in this study consisted of a syringe and needle (ID = 0.41 mm), a ground electrode, and a high voltage supply (Chungpa EMT Co., Republic of Korea). The needle was connected to the high voltage supply, which could generate positive DC voltages up to 40 kV. For the electrospinning of gelatin/CaP composite membranes, gelatin was first dissolved in a mixed solvent of TFE/distilled water at a volume ratio of 1:1 and then the CaP sol solution was mixed with different concentrations for 12 h. In the prepared electrospinning solutions, the concentration of gelatin was adjusted to 50 w/v% and the contents of CaP sol were 10, 20, 30 and 40 wt.% based on the weight of gelatin. Gelatin–CaP sol blend solution held in a 10 mL syringe was delivered into a needle spinneret by a syringe pump (KDS 100, KD Scientific Inc., USA) with a mass flow rate of 1.5 mL/h. The steel needle was connected to an electrode of a high voltage supply and a grounded stainless steel plate was placed at 12 cm distance from the needle tip to collect the fibers. The positive voltage applied to the polymer solutions was 15 kV. All experiments were carried out at room temperature and below 60% relative humidity (RH). After the electrospinning, the composite membrane was carefully peeled off from the stainless steel plate. The thermal treatment of the prepared electrospun composite membranes was next performed to prepare the hydroxyapatite (HA) nanofibers. All samples were pretreated at 200 °C for 1 h to stabilize the composite membranes. The elimination of gelatin from the electrospun composite membranes and the crystallization of HA were achieved by post-heating (sintering) under 400, 600 or 800 °C for 1 h

2.4. Characterization of hydroxyapatite nanofibers

The morphologies of HA nanofibers were observed by a field emission-scanning electronic microscope (FE-SEM, JSM-6335F, JEOL, Japan). Prior to SEM observation, all of the samples were coated with gold by low-vacuum sputter coating. The average diameter of nanofibers was determined by analyzing the SEM images with image analyzing software (Image-Pro Plus, Media Cybernetics Inc., USA). For the same samples of FE-SEM, the spectrum of energy dispersive X-ray spectroscopy (EDX) was applied to detect the CaP sol distribution profile on the electrospun membrane surface and to analyze the change of elemental composition of electrospun membranes due to the thermal treatment. Attenuated total reflectance Fourier transform infrared (ATR-FTIR) spectroscopy spectra of the samples were obtained with an ALPHA spectrometer (Brucker Optics, USA) in the wavenumber range 400–4000 cm^{-1}. X-ray diffraction (XRD) measurements were carried out to characterize the crystalline phase of HA nanofibers with a Panalytical X-ray diffractometer X'Pert Pro with Cu Kα radiation at 40 kV/30 mA. The diffractograms were scanned in a 2θ range of 20–60° at a rate of 2°/min. Ca/P molar ratio of HAs was analyzed with X-ray fluorescence spectroscopy (XRF, ZSX Primus II, Rigaku). The thermal stability of particles was evaluated by thermogravimetric analysis (TGA, Q500, TA Instruments, USA). The TGA measurements were carried out under nitrogen atmosphere at a heating rate of 5 °C/min from 30 to 800 °C, in which all of the samples were dried in vacuo at 50 °C for 48 h prior to the measurement.

2.5. Simulated body fluid immersion test

The formation of bone-like apatite on the surface of prepared HA nanofibers was examined in simulated body fluid (SBF) with ion concentrations nearly equal to those of human blood plasma [11]. The solution was prepared by dissolving reagent grade NaCl, $NaHCO_3$, KCl, $NaHPO_4 \cdot 2H_2O$, $MgCl_2 \cdot 6H_2O$, $CaCl_2 \cdot 2H_2O$,

Na_2SO_4 and $(CH_2OH)_3CNH_2$ into deionized water and titrated with 1 M HCl to the pH of 7.4 at 37 °C. Immersion studies were performed by incubating the HA nanofibers in 15 mL SBF solution in a Petri dish. All dishes were placed in a thermostatical shaking incubator (BioShaker MBR-022UP, Taitec Co.) at 37 °C. After 12 h, 1 day, and 3days, the HA nanofibers were gently washed with deionized water and dried in vacuo.

2.6. Cell viability assay

In vitro cytotoxicity of composite nanofibrous membranes was evaluated by a cell viability assay using mouse calvaria osteoblast cell line (MC3T3-E1). All cultures were made in MEM-α with 10% FBS and antibiotic/antimycotic in a humidified atmosphere under 5% CO_2 at 37 °C. When the cells reached 80% confluence, they were harvested by 0.25% trypsin–EDTA and seeded into a new tissue culture plate for subculture.

The cell viability onto composite membranes was investigated by the MTT assay. Prior to cell seeding, composite membranes were sterilized under UV for 3 h, followed by rinsing with PBS and a culture medium five times, respectively. Then, mouse calvaria osteoblasts (2×10^4 cells/well) were seeded on the composite membranes in a 24-well tissue culture plate and cultured for 1, 3, 5, and 7 days at 37 °C. To evaluate the cell viability, 0.2 mL of MTT solution (5 mg/mL in PBS) was added to the cultured cells, which were further incubated for 4 h at 37 °C. After removing the remaining medium, 1 mL of DMSO was added to each well to solubilize the precipitate. Then 0.2 mL of the resulting supernatant was transferred to a 96-well microplate and the optical density, which is proportional to the number of viable cells, was measured by a microplate reader (OPSYS-MR, Dynex Technology Inc.). The mechanism of this assay is that metabolically active cells react with tetrazolium salt in the MTT reagent to produce water-insoluble formazan dye that can be observed at 570 nm.

3. Results and discussion

3.1. Morphology of electrospun composite membranes

Electrospun membranes have recently gained much interest for bone tissue engineering, which have proved to be convenient and effective in providing mechanical support and osteoconductivity to the growing cells in bone regeneration [12,13]. Furthermore, ultrafine fibrous structures are thought to enhance cell adhesion, migration and proliferation. In this study, microfibrous composite membranes were first prepared by electrospinning from the gelatin–calcium phosphate (CaP) sol blend solutions containing different contents of CaP sol. The contents of CaP sol in the mixed solutions were 10 (GECP10), 20 (GECP20), 30 (GECP30) and 40 wt.% (GECP40) based on the weight of gelatin.

The morphological structure of the electrospun composite membranes is shown in Fig. 1. The resulting microfibers exhibited a fully interconnected pore structure. With increasing the concentration of CaP sol in the electrospinning solution, the average diameter of microfibers reduced, which was 1.44 ± 0.17 μm for GECP10, 1.32 ± 0.14 μm for GECP20, 1.21 ± 0.21 μm for GECP30 and 1.09 ± 0.24 μm for GECP40. This result may be related to the change of solution conductivity through the use of CaP sol. As shown in Fig. 2, the solution conductivity enormously increased from 2.23 mS/cm to 4.57 mS/cm by adding CaP sol. CaP is a member of a family of minerals containing calcium ions together with phosphate ions and shows decomposition behavior in wet environments under physiological condition to produce precursor ions. Aqueous polymer solutions including CaP sol have higher charge density on the surface of the ejected jet formed during electrospinning [9]. As the charges carried by the jet increase, higher elongation forces are imposed to the jet under the electrical field. It has been known that the overall tension in the fibers depend on the self-repulsion of the excess charges on the jet. Therefore, as the charge density increase, the fiber diameter becomes smaller [14].

The distribution of the CaP sol on the electrospun composite membranes was measured with the EDX. Fig. 3 presents the EDX Ca- and P-mapping analysis of electrospun GECP20 composite membrane. The bright spots representing Ca or P element clearly reflected a homogenous distribution of CaP sol on the membranes. In addition, high amount of CaP sol was detected on the composite membrane.

3.2. Properties of electrospun composite membranes

ATR-FTIR analysis was carried out for the surface characterization of pure gelatin, GECP10, GECP20, GECP30 and GECP40 electrospun membranes in the range of 400–4000 cm^{-1}. As shown in Fig. 4, pure gelatin membrane exhibited a characteristic absorption band at 3275 cm^{-1} associated with an N–H stretching vibration in gelatin. According to a previous report, a free N–H stretching vibration occurs in the range from 3400 to 3440 cm^{-1}, and when the N–H group of peptides is involved in hydrogen bonding, the position is shifted to lower frequencies, usually around 3300 cm^{-1} [15]. From this result, it seems that many of the N–H groups of gelatin are involved in intermolecular hydrogen bonding. In our experiments, the characteristic absorption band was slightly shifted from 3275 to 3290 cm^{-1} with increasing CaP sol content due to the reduction of intermolecular hydrogen bonding. In addition, common bands of gelatin appeared at approximately 1640 cm^{-1} (amide I) and 1540 cm^{-1} (amide II) in all samples, corresponding to the stretching vibration of C═O bond, and coupling of N–H bond bending and C–N bond stretching, respectively [16]. In the case of GECP composite membranes, new absorption bands for the vibrational mode of PO_4^{3-} of the CaP crystals appeared at around 1037 and 981 cm^{-1} as shown in Fig. 4 [2]. In addition, the band observed at 1410 cm^{-1} was attributed to the substitution of CO_3^{2-} ions in the place of PO_4^{3-} ions and confirmed the substitution of CO_3^{2-} in apatite structure. These CO_3^{2-} ions were formed by the reaction of CO_2 present in the atmosphere with OH^- ions of reaction medium. Furthermore, the absorption bands ascribed to NO_3^- of synthetic residuals were observed at 824 and 1340 cm^{-1} [17].

The thermal stability of composite membranes was investigated by means of TGA. Fig. 5 shows the typical TGA curve

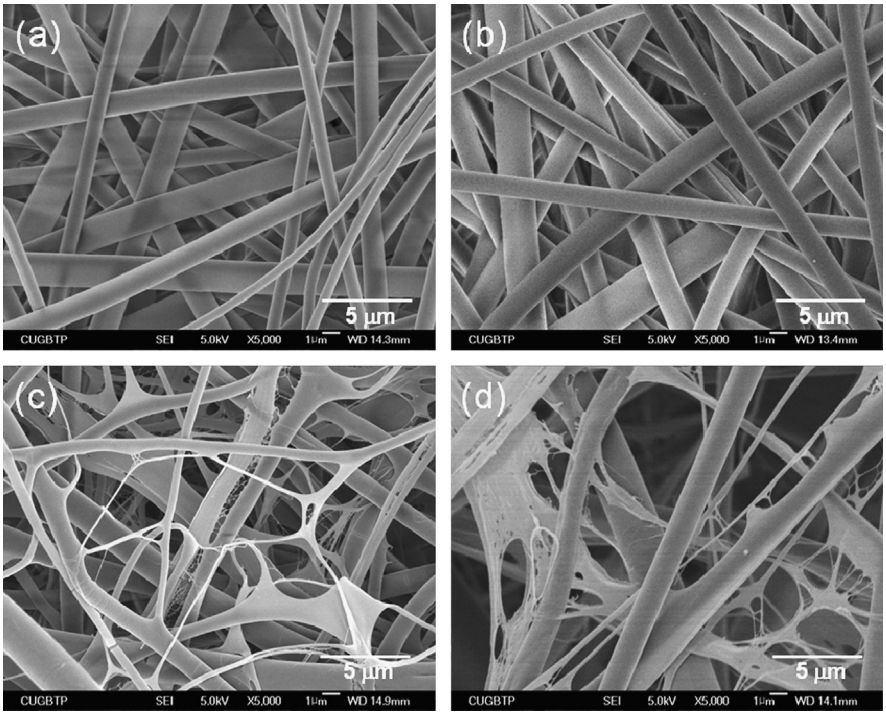

Fig. 1. SEM micrographs of (a) GECP10, (b) GECP20, (c) GECP30 and GECP40 composite membranes.

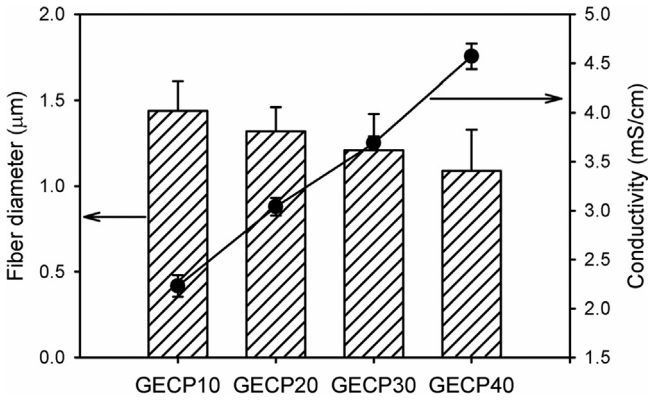

Fig. 2. Effect of the CaP sol concentration on the average fiber diameter of composite membranes and conductivity of the electrospinning solutions.

where the amount of weight loss is plotted against the temperature. Electrospun gelatin membrane exhibited a pattern of weight loss comprised of three main stages. The first stage of weight loss was observed over the temperature ranging from 30 °C to approximately 110 °C. This stage mainly was assigned to the evaporation of absorbed water. The second stage of weight loss started at around 240 °C, which was most likely imputed to the degradation or decomposition of gelatin [18]. Additionally, the third stage of weight loss in the temperature range of 360–580 °C is possibly attributed to the decomposition of higher interacted gelatin fractions. The weight loss pattern of GECP composite membranes was similar to that of pure gelatin membrane. The second step in temperature range of 170–370 °C is mainly due to the removal of crystalline water and synthesis residuals, and the decomposition of gelatin [18,19]. Additionally, the third step is possibly attributed to the release of CO_2 from $CaCO_3$ crystals formed by the isomorphous substitution of PO_4^{3-} by CO_3^{2-} during the synthesis of CaP sol (490–610 °C) [20]. According to the TGA data, the total weight loss at 800 °C reduced from 91.8% to 83.2% with the increase of CaP sol amount in the composite membranes.

3.3. Hydroxyapatite nanofibers

For the preparation of hydroxyapatite (HA) nanofibers, the thermal treatment of GECP20 composite membrane was carried out. GECP20 membrane was pretreated at 200 °C for 1 h for stabilization and then sintered at three different temperatures namely, 400, 600 and 800 °C for 1 h to study the process of HA crystallization. After the thermal treatment, the average fiber diameter of GECP20 membrane significantly reduced from 1.21 ± 0.21 μm to 400 ± 52 nm, which may be caused by the thermal elimination of gelatin and condensation of CaP sol as shown in Fig. 6. Moreover, the surface roughness of membrane increased with rising temperature by the formation of HA crystals through the gel reaction of CaP sol. However, the influence of thermal treatment temperature on the change of average fiber diameter was not observed.

ATR-FTIR analysis was performed to confirm the formation of HA nanofibers, which in turn provided information about the constitution and phase composition of the products thermal-treated with different temperature. The characteristic bands assigned to gelatin and synthetic residuals at around

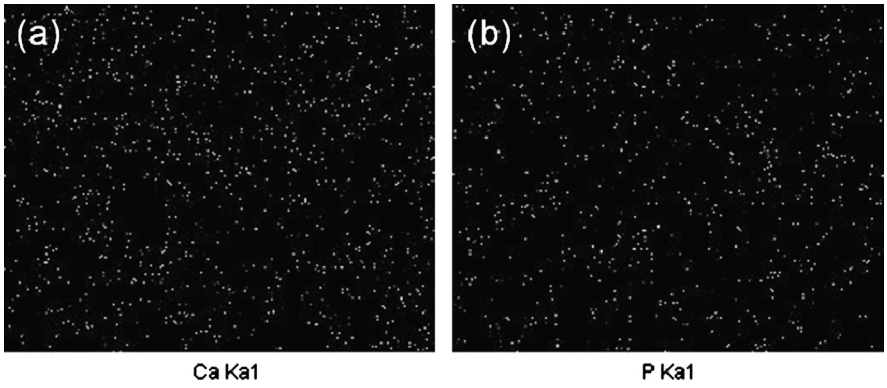

Fig. 3. EDX Ca- and P-mapping micrographs of GECP20 composite membrane.

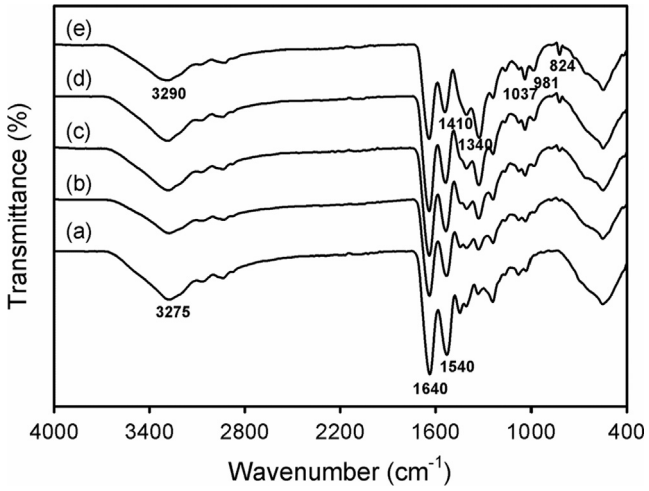

Fig. 4. ATR-FTIR spectra of (a) pure gelatin, (b) GECP10, (c) GECP20, (d) GECP30 and (e) GECP40 electrospun membranes.

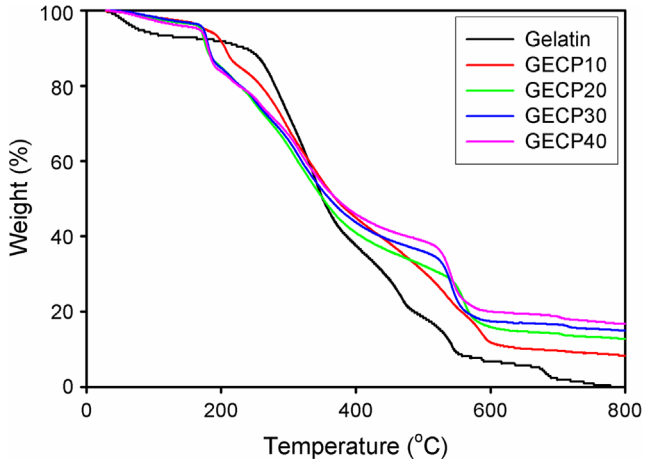

Fig. 5. TGA curves of (a) pure gelatin, (b) GECP10, (c) GECP20, (d) GECP30 and (e) GECP40 membranes.

3284, 1640, 1540, 1340 and 824 cm^{-1} clearly disappeared by the thermal treatment (Fig. 7). In addition, the absorption bands due to the formation of $CaCO_3$ crystals at 1420 and 870 cm^{-1} vanished after the thermal treatment at 800 °C. However, new bands for the vibrational modes of PO_4^{3-} appeared at around 1093, 1028, 984 and 566 cm^{-1}, and the band assigned to OH^- of HA was shown at 3630 and 640 cm^{-1} [17]. These data suggest that HA nanofibers are successfully produced by combining the electrospinning and thermal treatment methods in the sol–gel process.

To prove the production of HA nanofibers, the formation of HA crystals and the elimination of gelatin and synthetic residuals through the thermal treatment in the composite membranes were pursed with the EDX. As shown in Fig. 8, two peaks ascribed to carbon and nitrogen atoms of gelatin and synthetic residuals disappeared by the thermal treatment. Meanwhile, three peaks assigned to oxygen, phosphorous and calcium atoms of HA crystals increased with increasing the thermal treatment temperature, in agreement with the ATR-FTIR results [21].

The crystalline phases of the HA nanofibers were investigated by means of XRD (Fig. 9). GECP20 membrane exhibited amorphous phase until 400 °C, but the XRD patterns after the thermal treatment at 600 °C showed HA crystalline phase at around 24.9°, 28.3°, 31.2°, 33.5°, 39.1°, 46.0°, 47.4°, 48.8°, 49.6°, 50.4°, 51.3° and 53.3°, which reflected characteristic of the (002), (102), (211), (202), (310), (222), (312), (213), (321), (410), (402) and (004) planes [22]. However, all the peaks were broad diffraction peaks indicating a poorly crystallized HA phase because of the gelatin residuals. On the other hand, thermal-treated GECP20 membrane at 800 °C exhibited the diffraction peaks at around 25.2°, 28.2°, 31.1°, 32.2°, 33.4°, 34.8°, 39.1°, 41.4°, 46.1°, 47.4°, 48.8°, 49.8°, 50.5°, 51.3°, and 53.3°, which were imputed to the (002), (102), (211), (112), (202), (301), (310), (311), (222), (312), (213), (321), (410), (402) and (004) planes. This XRD pattern was exactly matched with the structural data of stoichiometric HA described in the Powder Diffraction File (JCPDS 09-432). The diffraction peaks were narrower than those of thermal-treated samples at low temperature, meaning the increment of crystallinity due to the elimination of gelatin and synthetic residuals. Previous study reported that the HA nanoparticles synthesized with alginate exhibited only a broad diffraction peak, indicating that the HA phase was poorly crystallized [23]. The HA nanoparticles subjected to thermal treatment at 800 °C displayed strong peaks that corresponded well to those of stoichiometric HA crystal, owing to the increase in crystallinity.

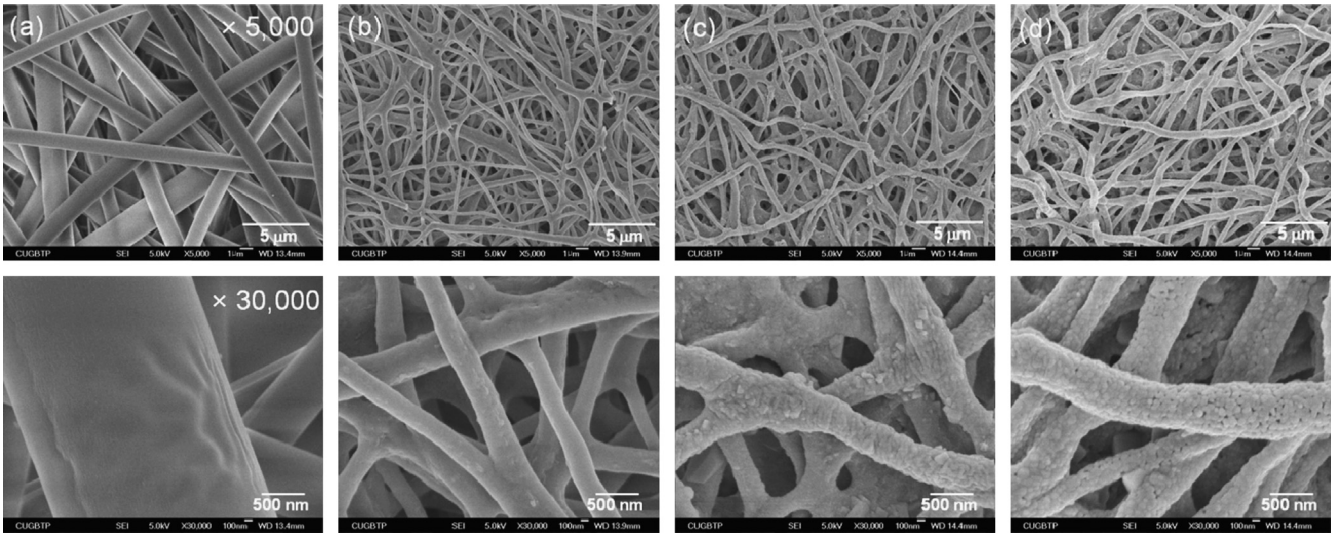

Fig. 6. SEM micrographs of thermal-treated GECP20 membranes with different temperature: (a) as-electrospun, (d) 400 °C, (c) 600 °C and (d) 800 °C.

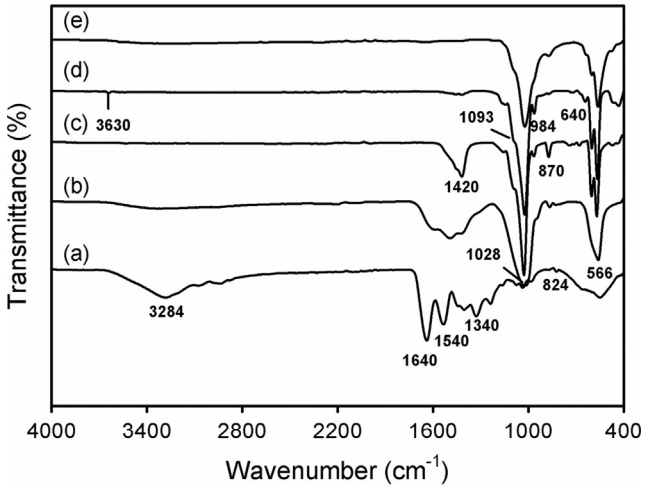

Fig. 7. ATR-FTIR spectra of (a–d) thermal-treated GECP20 membranes with different temperature and (e) commercial HA nanopowders: (a) as-electrospun, (b) 400 °C, (c) 600 °C and (d) 800 °C.

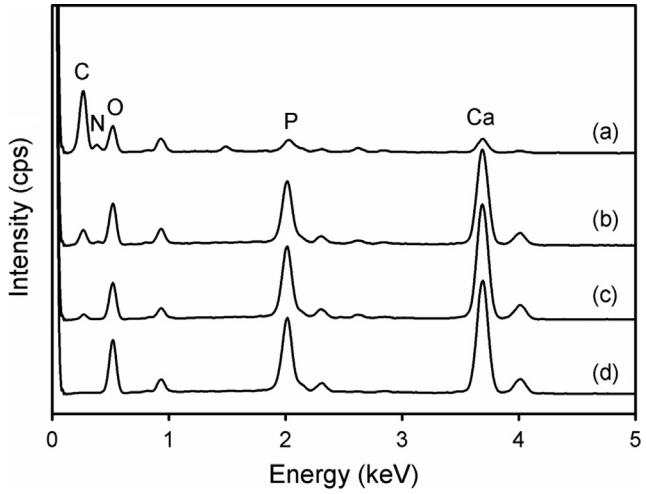

Fig. 8. EDX spectra of thermal-treated GECP20 membranes with different temperature: (a) as-electrospun, (b) 400 °C, (c) 600 °C and (d) 800 °C.

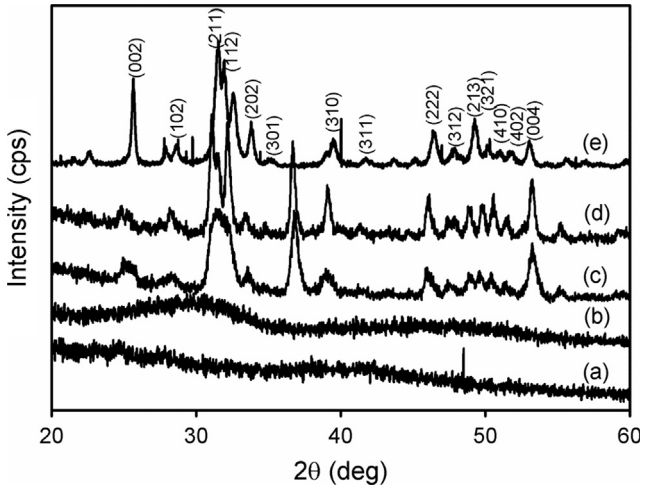

Fig. 9. X-ray diffraction patterns of (a–d) thermal-treated GECP20 membranes with different temperature and (e) commercial HA nanopowders: (a) as-electrospun, (b) 400 °C, (c) 600 °C and (d) 800 °C.

The Ca/P molar ratio of thermal-treated GECP20 membrane at 800 °C was determined by XRF, which was 1.68. This result means that stoichiometric HA nanofibers can be easily fabricated by combining the electrospinning and thermal treatment methods in the sol–gel process. Biomacromolecules containing polar functional groups such as COOH and OH have been found to be useful for the nucleation of apatite crystals in the solution because these side groups can form the intermolecular interaction with Ca^{2+} ions or PO_4^{3-} ions through coordination and hydrogen bonding and work on the crystallization process of biomineral materials [24].

3.4. Simulated body fluid immersion test

The essential requirement for an artificial material to bond to living bone is the formation of bone-like apatite on its surface when implanted in the living body, and that this in vivo apatite

formation can be reproduced in a simulated body fluid (SBF) with ion concentrations nearly equal to those of human blood plasma [11]. This means that the in vivo bone bioactivity of a material can be predicted from the apatite formation on its surface in SBF. After 12 h of immersion in SBF, the whole surface of the thermal-treated GECP20 membrane at 800 °C was fully covered by a layer of apatite consisted of nanosheets as shown in Fig. 10. Moreover, the underlying nanofibers of the membrane were not observable and the pores of membrane were clogged owing to considerable crystal growth after 3 days of immersion in SBF. On the other hand, the formation of bone-like apatite was hardly detected on the surface of thermal-treated GECP20 membrane at 400 °C after 12 h of immersion in SBF. After 3 days of mineralization in SBF, the whole surface of thermal-treated GECP20 membrane at 400 °C was covered by a layer of apatite. This result means that the HA nanofibers, thermal-treated GECP20 membrane at 800 °C, maybe reveals the improved in vivo bone bioactivity [13].

3.5. Cell viability assay

Tissue engineering scaffolding must promote cell growth and physiological function and should maintain normal states of cell differentiation. Thus the cytocompatibility of thermal-treated GECP20 membrane at 800 °C was examined as a potential candidate for scaffolds to be used in tissue engineering. An MTT assay was carried out to evaluate the cell viability of mouse calvaria osteoblasts (MC3T3-E1) on thermal-treated GECP20 membrane. MC3T3-E1 proliferated well on membrane during the incubation period (Fig. 11). Moreover, the number of attached cells in the early stage and cell proliferation on the GECP20 membrane were higher in comparison with tissue culture plate (TCP) control, indicating that HA has effectively accelerated the attachment and proliferation of MC3T3-E1 cells [12,13].

Cell morphology and the interaction between cells and nanofibers were also observed during the incubation period. SEM micrographs showed that MC3T3-E1 adhered and spread on the surface of HA nanofibers (Fig. 12). In addition, cell proliferation increased time-dependently, and cells were covering the entire GECP20 membrane and formed cell monolayer after 5 days of culture. This may be evidence of the ability of HA to stimulate the growth of MC3T3-E1. It is well known that HA materials exhibit excellent biocompatibility and have chemical compositions close to the bone mineral, which are suitable for biomedical applications [1,2].

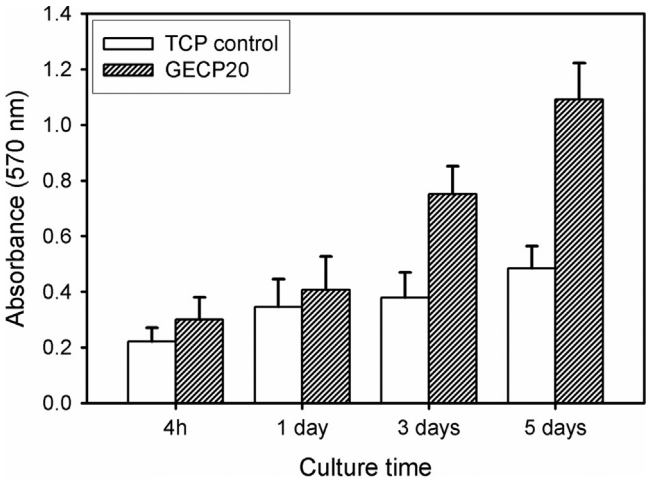

Fig. 11. Cell viability of MC3T3-E1 cells incubated onto thermal-treated GECP20 membrane at 800 °C as a function of culture time.

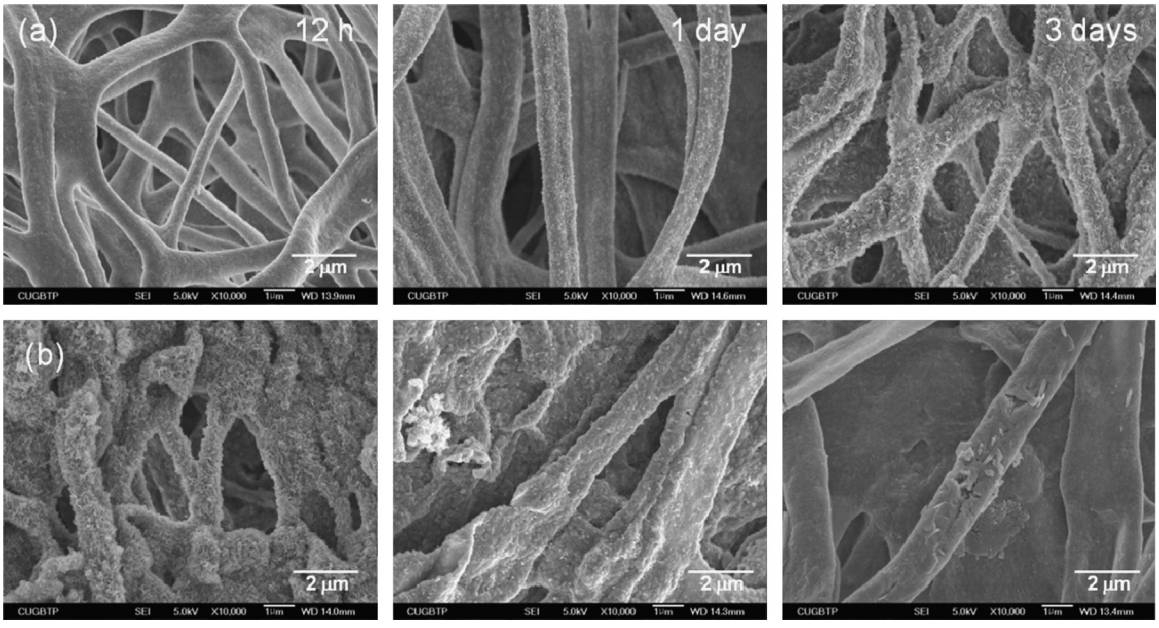

Fig. 10. SEM micrographs of thermal-treated GECP20 membranes at (a) 400 °C and (b) 800 °C after immersion in SBF for different periods of time (12 h, 1 day and 3 days).

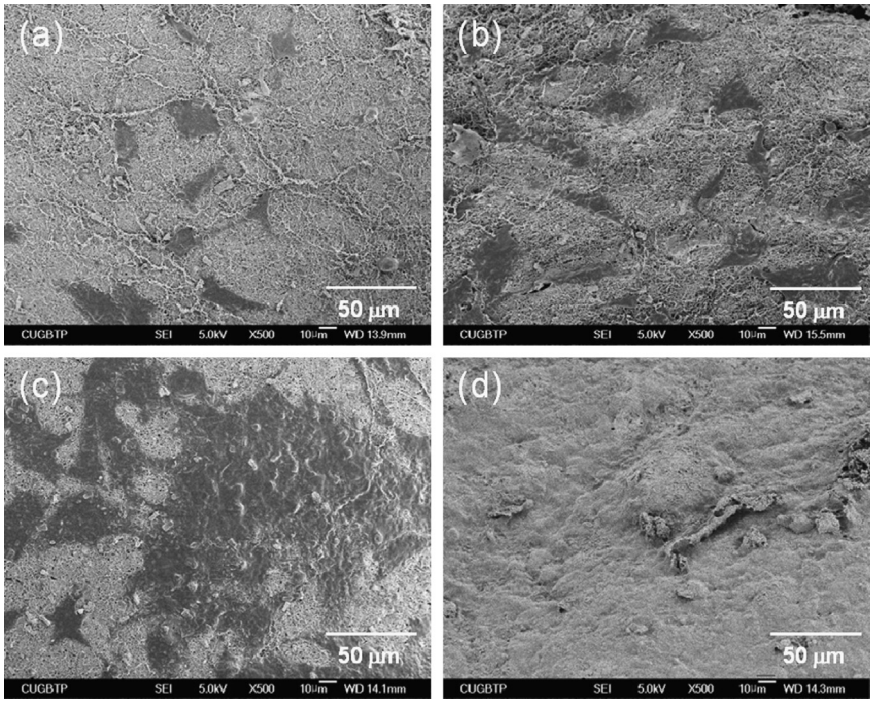

Fig. 12. SEM micrographs of MC3T3-E1 cells grown on thermal-treated GECP20 membrane at 800 °C after (a) 4 h, (b) 1 day, (c) 3 days and (d) 5 days.

4. Conclusions

In recent years, the HA nanofibers have been crucial in biomedical applications. Their structural characteristics are necessary to enhance the cell attachment and to expedite the tissue in growth both in vitro and in vivo. In this study, the HA nanofibers were prepared by combining the electrospinning and thermal treatment methods in the sol–gel process. Microfibrous composite membranes were first prepared by electrospinning from the gelatin–CaP sol blend solutions. After sintering at 800 °C, nano-sized HA fibers were obtained and these nanofibers showed a porous morphology formed by interlaying of the fibers. The composition and crystalline phase were similar to those of the stoichiometric HA. The resulting HA nanofibers have effectively accelerated the attachment and proliferation of MC3T3-E1 cells. It is concluded that this new method for making the HA nanofibers may be helpful to develop optimized artificial bone materials.

Acknowledgments

This research was financially supported by the "Advanced Medical Material (Fiber) Development Program" through the Ministry of Trade, Industry & Energy (MOTIE) and Korea Institute for Advancement of Technology (KIAT).

References

[1] H. Zhou, J. Lee, Nanoscale hydroxyapatite particles for bone tissue engineering, Acta Biomaterialia 7 (2011) 2769–2781.
[2] F. Scalera, F. Gervaso, K.P. Sanosh, A. Sannino, A. Licciulli, Influence of the calcinations temperature on morphological and mechanical properties of highly porous hydroxyapatite scaffolds, Ceramics International 39 (2013) 4839–4846.
[3] G. Devanand Venkatasubbu, S. Ramasamy, G.S. Avadhani, V. Ramakrishnan, J. Kumar, Surface modification and paclitaxel drug delivery of folic acid modified polyethylene glycol functionalized hydroxyapatite nanoparticles, Powder Technology 235 (2013) 437–442.
[4] C.B. Carter, M.G. Norton, Ceramic Materials: Science and Engineering, Springer, New York, 2007.
[5] C. Chang, N. Peng, M. He, Y. Teramoto, Y. Nishio, L. Zhang, Fabrication and properties of chitin/hydroxyapatite hybrid hydrogels as scaffold nano-materials, Carbohydrate Polymers 91 (2013) 7–13.
[6] O. Lyckfeldt, J.M.F. Ferreira, Processing of porous ceramics by 'starch consolidation, Journal of the European Ceramic Society 18 (1998) 131–140.
[7] P. Sepulveda, J.G.P. Binner, Evaluation of the in situ polymerization kinetics for the gelcasting of ceramic foams, Chemistry of Materials 13 (2001) 3882–3887.
[8] S.H. An, T. Matsumoto, H. Miyajima, A. Nakahira, K.H. Kim, S. Imazato, Porous zirconia/hydroxyapatite scaffolds for bone reconstruction, Dental Materials 28 (2012) 1221–1231.
[9] P.Q. Franco, C.F.C. João, J.C. Silva, J.P. Borges, Electrospun hydroxyapatite fibers from a simple sol–gel system, Materials Letters 67 (2012) 233–236.
[10] Y.J. Kim, C.H. Ahn, M.O. Choi, Effect of thermal treatment on the characteristics of electrospun PVDF–silica composite nanofibrous membrane, European Polymer Journal 46 (2010) 1957–1965.
[11] T. Kokubo, Bioactive glass ceramics: properties and applications, Biomaterials 12 (1991) 155–163.
[12] M.E. Frohbergh, A. Katsman, G.P. Botta, P. Lazarovici, C.L. Schauer, U.G. Wegst, P.I. Lelkes, Electrospun hydroxyapatite-containing chitosan nanofibers crosslinked with genipin for bone tissue engineering, Biomaterials 33 (2012) 9167–9178.
[13] A. Abdal-hay, H.R. Pant, J.K. Lim, Super-hydrophilic electrospun nylon-6/hydroxyapatite membrane for bone tissue engineering, European Polymer Journal 49 (2013) 1314–1321.
[14] Y.T. Jia, J. Gong, X.H. Gu, H.Y. Kim, J. Dong, X.Y. Shen, Fabrication and characterization of poly (vinyl alcohol)/chitosan blend nanofibers produced by electrospinning method, Carbohydrate Polymers 67 (2007) 403–409.

[15] T. Nagai, N. Suzuki, T. Nagashima, Collagen from common minke whale (*Balaenoptera acutorostrata*) unesu, Food Chemistry 111 (2008) 296–301.
[16] N. Zhang, X. Liu, L. Yu, R. Shanks, E. Petinaks, H. Liu, Phase composition and interface of starch–gelatin blends studies by synchrotron FTIR micro-spectroscopy, Carbohydrate Polymers 95 (2013) 649–653.
[17] S. Raynaud, E. Champion, D. Bernache-Assollant, P. Thomas, Calcium phosphate apatites with variable Ca/P atomic ratio I. Synthesis, characterization and thermal stability of powders, Biomaterials 23 (2002) 1065–1072.
[18] M.S. Hoque, S. Benjakul, T. Prodpran, P. Songtipya, Properties of blend film based on cuttlefish (*Sepia pharaonis*) skin gelatin and mungbean protein isolate, International Journal of Biological Macromolecules 49 (2011) 663–673.
[19] K. Mahmud, A. Mitsionis, T. Vaimakis, N. Kourkoumelis, C. Trapalis, The threonine effect on calcium phosphate preparation from a solution containing Ca/P = 1.33 M ratio, Ceramics International 36 (2010) 1893–1899.
[20] M.C. Chang, C. Ko, W.H. Douglas, Preparation of hydroxyapatite–gelatin nanocomposite, Biomaterials 24 (2003) 2853–2862.
[21] E. Kusrini, M. Sontang, Characterization of X-ray diffraction and electron spin resonance: effects of sintering time and temperature on bovine hydroxyapatite, Radiation Physics and Chemistry 81 (2012) 118–125.
[22] X.F. Xiao, R.F. Liu, C.F. Qiu, D.C. Zhu, F. Liu, Biomimetic synthesis of micrometer spherical hydroxyapatite with β-cyclodextrin as template, Materials Science and Engineering C 29 (2009) 785–790.
[23] K.D. Son, D.J. Yang, M.S. Kim, I.K. Kang, S.Y. Kim, Y.J. Kim, Effect of alginate as polymer matrix on the characteristics of hydroxyapatite nanoparticles, Materials Chemistry and Physics 132 (2012) 1041–1047.
[24] M. Okada, S. Fujii, T. Nishimura, Y. Nakamura, S. Takeda, T. Furuzono, Solvent-free formation of hydroxyapatite coated biodegradable particles via nanoparticle-stabilized emulsion route, Applied Surface Science 262 (2012) 39–44.